Analysis of FBG reflection spectra under uniform and non-uniform transverse loads

Fazzi, Luigi; Rajabzadeh, Aydin; Milazzo, Alberto; Groves, Roger M.

DOI
10.1117/12.2513795

Publication date
2019

Document Version
Final published version

Published in
Sensors and Smart Structures Technologies for Civil, Mechanical, and Aerospace Systems 2019

PROCEEDINGS OF SPIE

SPIEDigitalLibrary.org/conference-proceedings-of-spie

Analysis of FBG reflection spectra under uniform and non-uniform transverse loads

Luigi Fazzi, Aydin Rajabzadeh, Alberto Milazzo, Roger M. Groves

Luigi Fazzi, Aydin Rajabzadeh, Alberto Milazzo, Roger M. Groves, "Analysis of FBG reflection spectra under uniform and non-uniform transverse loads," Proc. SPIE 10970, Sensors and Smart Structures Technologies for Civil, Mechanical, and Aerospace Systems 2019, 109701X (27 March 2019); doi: 10.1117/12.2513795

SPIE.

Event: SPIE Smart Structures + Nondestructive Evaluation, 2019, Denver, Colorado, United States

Analysis of FBG reflection spectra under uniform and non-uniform transverse loads

Luigi Fazzi*[a,b], Aydin Rajabzadeh[a,c], Alberto Milazzo[b], Roger M. Groves[a]
[a]Structural Integrity and Composites group of Faculty of Aerospace Engineering, Department of Delft University of Technology, Delft, 2629 HS, The Netherlands
[b]Faculty of Aerospace Engineering of Palermo University, Palermo, Viale delle Scienze 90133, Italy
[c]Circuits and Systems group, Delft University of Technology, Delft, 2628 CD, The Netherlands

ABSTRACT

Loads applied transversely on the external surface of waveguides change their circular cross-sectional geometry generating birefringence. Due to this effect the reflected spectrum of a Fibre Bragg grating (FBG) undergoes a splitting of the single peak of the Bragg wavelength. In this work, we employed the Transfer Matrix Method (TMM) for x- and y-polarized wave-modes to model the uniform FBG reflection spectra for uniform and non-uniform transverse loads. We also performed experimental measurements for two different transverse load scenarios. The load profiles chosen for these experiments were applied on the FBG sensor through a block of steel and a roll bearing pin. Then, the modelled and experimental results were compared resulting in good agreement of 85% (on average). Finally, during the roll bearing pin loading test, different responses were observed depending how the FBGs were surface mounted. To investigate this, the glue layer influence on the reflected spectrum was further studied experimentally.

Keywords: uniform FBG, birefringence, transverse loads, transfer matrix, Structural Health Monitoring (SHM), polarization.

1. INTRODUCTION

Fibre optic sensors have distinct properties that make them interesting in aeronautical applications, including their insensitivity to electromagnetic interferences and an operational life similar to that of aerospace composite materials [1]. Furthermore, the morphology of fibre optics, although an order of magnitude larger in diameter, is quite similar to that of the reinforcement fibres in aeronautical composite structures. This and their small intrusiveness make them suitable to be embedded between the layers of composite materials. A specific type of fibre optic sensor is the fibre Bragg grating (FBG) sensor, which is produced by creating a spatial modulation in the refractive index of the core of the optical fibre [2]. The length of this modulation, usually ranging from 1 mm to a few centimeters, reflects a narrow wavelength spectrum of the input light. This reflected beam comes from the coupling between counter-propagating modes along the core of fibre. The spectral peak reflected from the grating is at the Bragg wavelength (λ_B), which is characterized by [2]

$$\lambda_B = 2n_{eff}\Lambda \qquad (1)$$

where n_{eff} is the effective refractive index of the core, and Λ is the grating period. It can be seen from (1) that a uniform axial strain applied over the length of the sensor will result in a linear shift of the Bragg wavelength. Following this equation, an elongation of the Bragg grating imposes a red shift of the reflected peak, while the peak moves towards blue wavelengths for compression. Hence, the information given by the FBG is wavelength-encoded. This allows the sensor to be self-referencing, insensitive to light irradiance fluctuations and to perform measurements absolutely independent from the illumination source. For all these reasons, the use of FBGs as strain sensors has been amply studied, and there exists an extensive scientific literature in the field of FBGs for aeronautical applications [3].
However, under transverse loads, the interpretation of the FBG reflection spectra become more complicated. Indeed, external transverse loads induce birefringence in the optical fibre, which is a result of polarization changes of the light beam propagating in the fibre core. In the absence of an external transverse load, non-birefringent fibre optics can be considered to be isotropic dielectric waveguides with a circularly symmetric refractive index distribution along their diameter, and perfectly circular cross-sections [4]. When a uniform transverse load is applied over the length of an optical

*l.fazzi@tudelft.nl

Sensors and Smart Structures Technologies for Civil, Mechanical, and Aerospace Systems 2019, edited by Jerome P. Lynch, Haiying Huang, Hoon Sohn, Kon-Well Wang, Proc. of SPIE Vol. 10970, 109701X

fibre, the cross-section of the fibre changes from being circular to an elliptic form. Under such conditions, due to the geometrical changes and the anisotropy of the material, the effective refractive index is different along the two polarizations axes of the light. Due to the photoelastic properties of the fibre optic material, it is possible to calculate $n_{eff\,x}$ and $n_{eff\,y}$ for the x- and y-polarization axes [4]. Moreover, the stress distribution along the x- and y-axes could also be different, which would result in two different propagation constants for the propagating modes in the x- and y-directions. Under these conditions the coupling, and consequently, an energy exchange between different propagation modes in the optical fibre can take place. When an FBG is placed under uniform transverse loads, this birefringence presents itself as the splitting of the reflection peak into two well-defined peaks whose corresponding Bragg wavelengths are different [4,5,6]. The focus of this paper is on the development of a numerical method to analyze the behavior of commercial uniform FBG sensors under different uniform and non-uniform transverse loads. Computer simulations and experimental measurements were used to validate the model, in which two different loading scenarios were investigated. The next section deals with the theory of FBG birefringence starting from the Coupled Mode theory and applying the TMM to get the reflections for slow and fast polarization axes. In the third section we introduce the experimental setup used to perform the tests, while in section number four the simulation and experimental results are shown and discussed. Summary conclusions deriving from the simulations and empirical tests regarding the behavior of FBG sensors when subjected to transverse loads have been included in the fifth section.

2. THEORY OF FBG BIREFRINGENCE

In the following treatment, we consider as negligible the possible weak linear birefringence induced during the writing of the Bragg grating in the fibre optic as modern techniques for low birefringence FBG manufacturing are well able to minimize this effect. Now, suppose a transverse load F is applied on an FBG sensor, as shown in Fig. 1, with the assumption that the load coincides with the main birefringence axes (fast and slow).

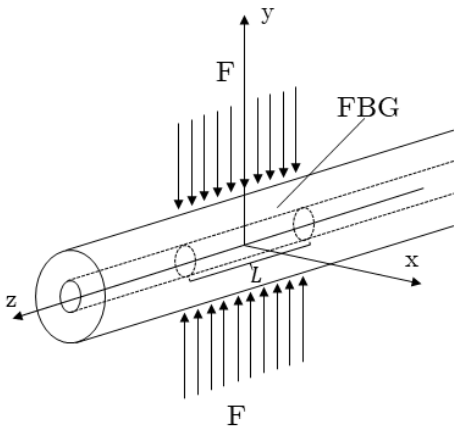

Fig. 1. Optical fibre affected by a transverse load and the reference system.

To obtain the FBG reflected spectrum in this condition, it is necessary to calculate the change in the effective refractive index, in the x- and y-polarization axes. The values of the effective indices can be calculated for both the polarization axes by using Gafsi's formulas [7]. The stresses induced in the dielectric material of the waveguide by the load were analytically investigated by Gianino and Bendow [8]. Substituting the values of the effective refractive indices in equation (1) we get two different Bragg wavelengths corresponding to the peaks of the polarization axes. Hence, the reflectance spectrum of a uniform FBG undergoing a transversal load is affected by the split of the reflection peak. However, the variation of the Bragg wavelength for slow and fast axes depends on the elastic-optic tensor of the material and the stress/strain state induced by the loads [4,8]. We can calculate these variations in each cross-sectional area's point P(x,y,z) of our Bragg grating:

$$\Delta\lambda_{B_x}(x,y,z) = \lambda_B \left[\varepsilon_z - \frac{{n_{eff_x}}^2}{2} \left[p_{11}\varepsilon_x + p_{12}(\varepsilon_y + \varepsilon_z) \right] \right], \quad (2)$$

$$\Delta\lambda_{B_y}(x,y,z) = \lambda_B \left[\varepsilon_z - \frac{{n_{eff_y}}^2}{2} \left[p_{11}\varepsilon_y + p_{12}(\varepsilon_x + \varepsilon_z) \right] \right], \quad (3)$$

where p_{11} and p_{12} are the strain-optic coefficients of the elastic-optic tensor, and $\varepsilon_x(x,y,z)$, $\varepsilon_y(x,y,z)$, $\varepsilon_z(x,y,z)$ are the strain components. Equations (2) and (3) can be also written in terms of stress using the stress-strain relationships for linear elastic materials.

The Bragg grating structure was written in monomode optical fibre, therefore only one propagating mode is related to reflection and one to transmission spectrum. Therefore only the fundamental linearly polarized mode LP_{01} is used in the formulation of the Coupled Mode theory equations. The latter are differential equations describing the coupling of modes inside the waveguides whose amplitudes are $A(z)$ and $B(z)$. For a uniform FBG affected by birefringence, the equations can be written for both the polarization axes [4] as below:

$$\begin{aligned}\frac{dA_{x,y}(z)}{dz} &= i\,\kappa_{x,y}\,B_{x,y}(z)\cdot\exp\left[2i\left(\Delta\beta_{x,y}\right)z\right]+g_g A_{x,y}(z),\\ \frac{dB_{x,y}(z)}{dz} &= i\,\kappa^{*}_{x,y}\;A_{x,y}(z)\cdot\exp\left[-2i\left(\Delta\beta_{x,y}\right)z\right]-g_g B_{x,y}(z).\end{aligned} \tag{4}$$

In the above equations, the subscript $(\cdot)_{x,y}$ indicates that similar relations hold for both x (slow) and y (fast) polarization directions, while z is the direction along the longitudinal axis of the fibre optic (Fig. 1). Also, g_g is the gain for a unit of length, $\Delta\beta_{x,y}$ and defines the difference in the propagation constants of the forward and backward electric waves for x- and y-polarized modes, $\kappa_{x,y}$ is the coupling mode coefficient and $\kappa^{*}_{x,y}$ its conjugate. The coupling coefficient determines the mutual coupling between the backward mode and the forward mode as an exchange of energy between the two [9].

The Coupled-Mode theory equations can be solved analytically or using numerical techniques. We used the TMM [10], one of the most common numerical approaches to analyze the reflected spectrum coming from the FBG affected even by non-uniform loads. This numerical technique consists of dividing the length L of the sensor into N piece-wise uniform sections of length $\Delta = L/N$ (Fig. 2), calculating the reflected and the transmitted electric waves in each of these segments, and finally, calculating the overall reflected and transmitted spectra of the whole sensor. Assuming the continuity conditions apply to the forward and backward waves at the interface of any two consecutive segments, the basis of the method consists of connecting the forward (E_{A_i}) and backward (E_{B_i}) electric waves of each two consecutive segments of the FBG through appropriate transfer matrices.

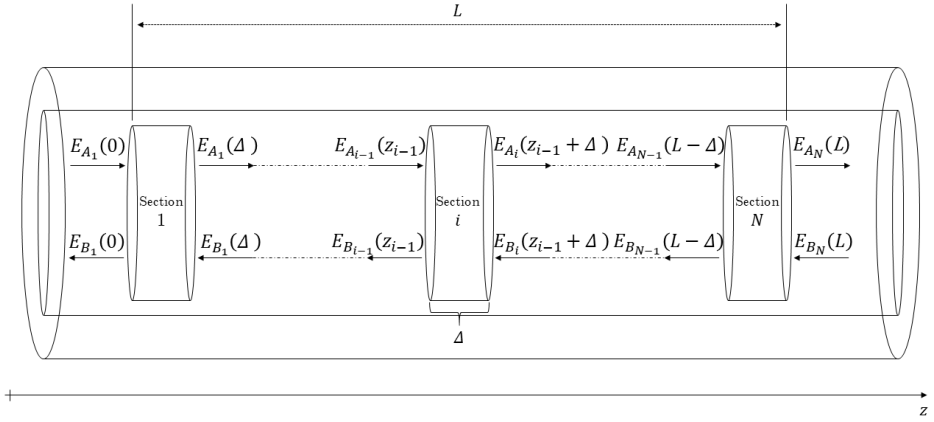

Fig. 2. Schematic of TMM's sub-gratings system.

In our case of polarized light, or birefringence induced in the FBG, this model can incorporate both, slow and fast, polarization directions of the electric waves. Solving equation (4) and considering the boundary conditions, the exact solution can be written for each sub-segment of Bragg grating is:

$$\begin{bmatrix}E_{A_i}(z+\Delta)\\ E_{B_i}(z+\Delta)\end{bmatrix}_{x,y} = T_{x,y_i}\begin{bmatrix}E_{A_i}(z)\\ E_{B_i}(z)\end{bmatrix}_{x,y}. \tag{5}$$

Where T_{x,y_i} is the transfer matrix of each i-th segment:

$$T_{x,y_i} = \begin{bmatrix}\cosh\left(\gamma_{x,y_i}\Delta\right) - i\frac{\Delta\beta_{x,y_i}}{\gamma_{x,y_i}}\sinh\left(\gamma_{x,y_i}\Delta\right) & -\frac{\kappa_{x,y_i}}{\gamma_{x,y_i}}\sinh\left(\gamma_{x,y_i}\Delta\right)\\ i\frac{\kappa_{x,y_i}}{\gamma_{x,y_i}}\sinh\left(\gamma_{x,y_i}\Delta\right) & \cosh\left(\gamma_{x,y_i}\Delta\right) + i\frac{\Delta\beta_{x,y}}{\gamma_{x,y_i}}\sinh\left(\gamma_{x,y_i}\Delta\right)\end{bmatrix}. \tag{6}$$

The components of transfer matrix are the same as equation (4), which, in the case of uniform FBG, are defined for each i-th segment and both polarization axes as below:

$$\Delta\beta_{x,y_i} = 2\pi\, n_{eff_{x,y_i}} \left(\frac{1}{\lambda} - \frac{1}{\lambda_{B_{x,y_i}}}\right), \tag{7}$$

$$\kappa_{x,y_i} = \frac{\pi}{\lambda_{B_{x,y_i}}} \delta n\, \upsilon\, g(z), \tag{8}$$

$$\gamma_{x,y_i} = \sqrt{\kappa_{x,y_i}{}^2 - \Delta\beta_{x,y_i}{}^2}. \tag{9}$$

Where λ is the wavelength range under investigation, $\lambda_{B_{x,y_i}}$ is the local Bragg wavelength of the i-th segment, δn is the 'ac' refractive index modulation of the core, υ is the fringe visibility and $g(z)$ is the apodizing function. Since the FBG is uniform and without apodization ($g(z) = 1$), we can consider $\upsilon = 1$ [11]. Once each i-th sub-section matrix is known, we can link the electromagnetic field at the ends of the sensor by multiplying all the matrices as follows

$$T_{x,y} = T_{N_{x,y}} \cdot T_{N-1_{x,y}} \cdot \ldots \cdot T_{i_{x,y}} \cdot \ldots \cdot T_{1_{x,y}}, \tag{10}$$

to obtain the global transfer matrix. This allows the first and the last segments of the FBG to be related for both polarization axes. The FBG reflection spectrum is defined as the sum of the two polarization components of the reflected light, i.e. $R = R_x + R_y$ [4]. Hence, assuming that there is full transmission ($E_{A_i}(L) = 1$) and zero reflection ($E_{B_i}(L) = 0$) at the end of the last segment of the FBG structure, the total reflection spectrum can be calculated as

$$R(\lambda) = \left(\frac{T_{21_x}}{T_{11_x}}\right)^2 + \left(\frac{T_{21_y}}{T_{11_y}}\right)^2, \tag{11}$$

in which each component T_{ij} is the (i,j)'th element of the T matrix calculated in (10).

The TMM, applied to FBG reflection spectrum modeling, is a powerful numerical tool because once the global transfer matrix of the FBG is defined, it allows the spectra to be obtained for any load condition. Especially in our work, this method is effective as it allows the application of different load values to each sub-segment of the Bragg grating. By increasing the number of sub-segments, the FBG spectrum can be simulated considering any axial and transverse load profile. However, there exists a limit number of sub-segments in which the grating can be divided, this limitation is determined by the required calculation accuracy [12]. In order to guarantee the efficiency of the Coupled-Mode theory, the number of sub-sections should be too large, that is less than the ratio between two times the effective refractive index and the Bragg wavelength. In other words, the axial length of each sub-grating has to be larger than the grating period, which is the distance between two adjacent Bragg grating planes.

3. EXPERIMENTAL SETUP

This section deals with the setup used to perform the experiments. The aim is to obtain the reflected spectra of FBG sensors that undergo to the same load conditions of the numerical simulations for mutual comparison. Specially, the condition of uniform transverse load was compared between the numerical and experimental results. For the experiments in this study, we used SG-01 type sensors (FBGS International NV), with an active length of 8 mm and nominal Bragg wavelengths of 1540 nm and 1560 nm. For the sake of comparison, similar characteristics were set for the simulated sensors. The experimental setup for the first scenario is shown in Fig. 3, where the fibre containing the FBG sensor was surface mounted on an aluminum 6082 alloy plate, and a supporting optical fibre was placed parallel to it to provide a second support line to the block so that the transverse load remains (relatively) uniform along the length of the sensor. The applied force was adjusted by means of a screw clamp (81785 VISE, Alufix). However, in order to apply a uniform load on the FBG, a steel block was used to transfer load between the clamp and the fibre optic. The FBG sensor and the steel block were placed, one over the other, in correspondence of the transverse midline of the aluminum plate. For the second experiment scenario, the transverse load was applied on the FBG through a roll bearing pin, this allows a non-uniform profile of transverse load to be imposed. In this context the optical fibre used as support can be removed and two different kinds of experiments were performed. In the first experiment, the load was imposed on the FBG sensor glued on the surface of the plate, while in the

second one the pin acts on the bare FBG which was kept in straight-position through layers of glue tape fixed on the optical fibre ends.

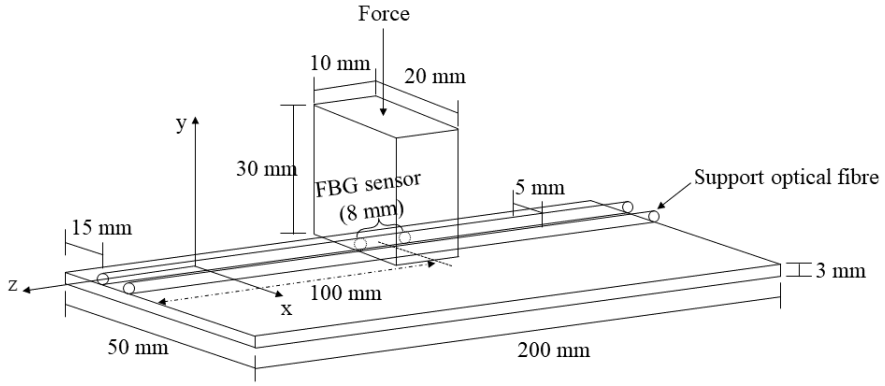

Fig. 3. Schematic of the first experimental setup.

For both the load profiles applied through the block and the pin, the amplitude of the transverse load imposed by the clamp on the FBG sensor along the axial (z-), lateral (x-) and transverse (y-) directions was measured using a 3D force sensor (OptoForce® OMD). The values of the load along the three directions allows the alignment of the components forming the experimental setup to be checked. Moreover, a bad alignment could modify the fibre in-plane force state, which it could mean unknown tensile or compression strains along the fibre optic. About data acquisition, the FBG reflected spectra were recorded using the PXIe-4844 interrogator (National Instruments), which provides a wavelength resolution of 4 pm with accuracy of 1 pm, while the amplitude resolution is 0.001 dB (worst case). Figure 4 shows the operating scheme of the experimental setup, through a laptop the Optoforce sensor software monitored the induced force by the clamp, while, in meantime the FBG spectra were recorded by a dedicated LabVIEW program.

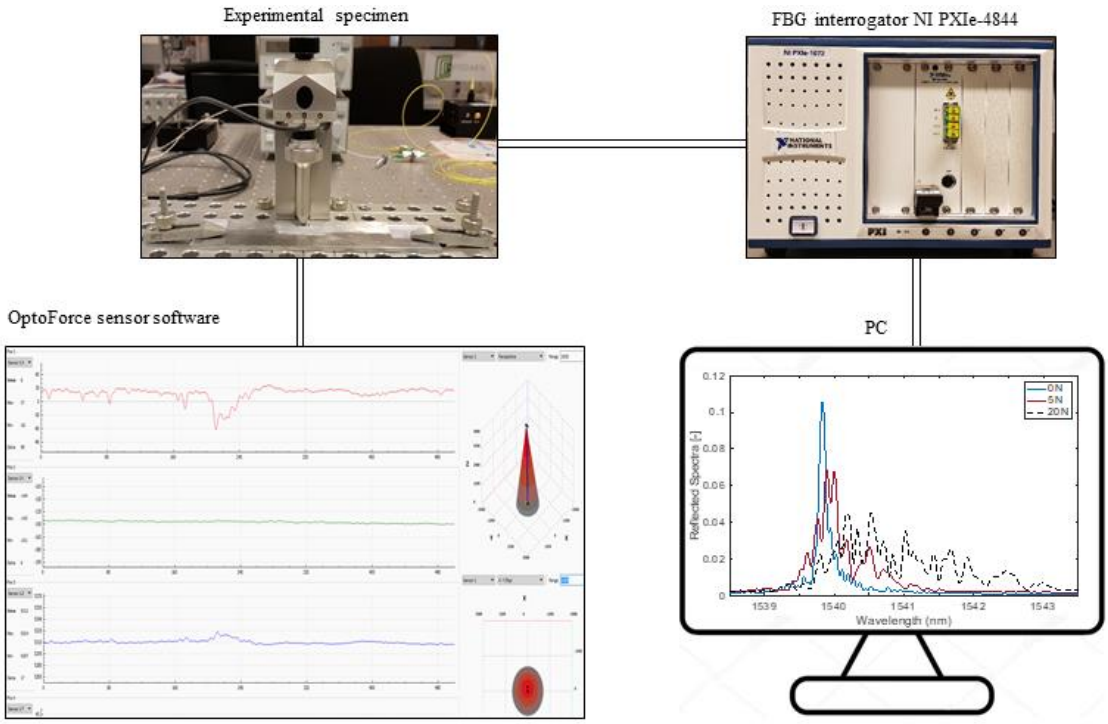

Fig.4. Diagram of the general laboratory setup used in the experiments.

4. RESULTS AND DISCUSSION

We used the model presented in Section 2 to investigate the FBG reflection spectra in response to uniform and non-uniform transverse forces. Hence, the steel block was used initially to investigate the effect of the uniform transverse loads, while successively we used the roll bearing pin to induce a non-uniform load profile on the FBG. For the first scenario, computer simulations were developed to analyze the behavior of FBG reflection spectra under different uniform transverse forces and the model results were compared with experimental results for similar loadings. The simulation results of such a sensor under different transverse loads, determined using the mathematical model presented in Section 2 are shown in Fig. 5a, and the experimental reflected spectra are presented in Fig. 5b. In the spectra the left peak is the slow polarization axis, while the peak on the right is the fast one. Due to the manufacturing imperfections of real FBG sensors and the inaccuracies associated with the experimental setup, the morphology of the reflected spectra in the simulations and the experiments do not correspond very well. However, in both the results, it is possible to note that as the load increases, the splitting of the reflected peak becomes increasingly pronounced, shifting towards greater wavelengths, which is in accordance with the transfer matrix model. The FBG spectra acquired during the tests in the lab show a further effect, the amplitude of the reflected peaks decreases with the growing of the transverse load. We believe this effect happens due to the reduction of the core cross-section in which the propagating light is reflected by the Bragg grating. Since the effect of crushing of the load on the sensor increasingly ovalizes the optical fibre core, the section of the Bragg grating suitable for the reflection of light becomes smaller, which translates into a lowering amount of light that the sensor is reflecting, that means a reduction of peak amplitude. This effect is not taken into account by the mathematical model described in section 2, however, this is not a limitation to our aim because the information about the external perturbation are given by the FBG sensor wavelength encoded.

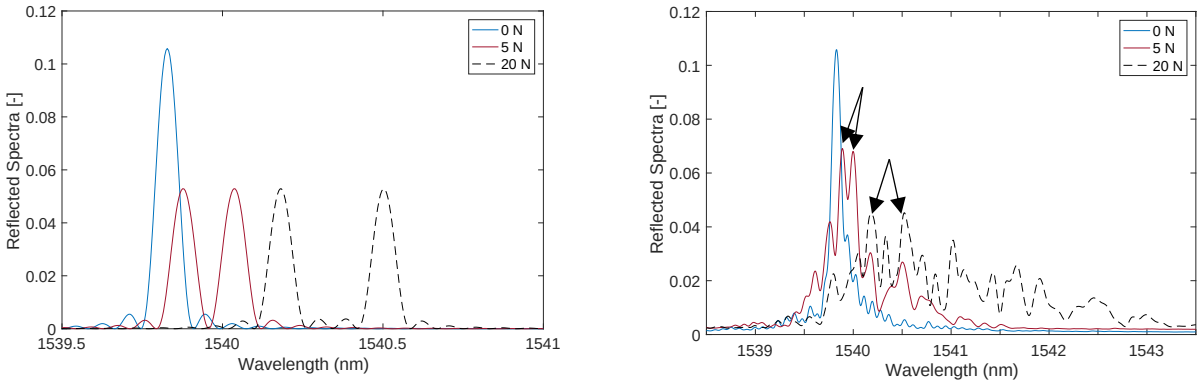

Fig. 5. Reflected spectra from (a) computer simulations, and (b) the experiment using a steel block.

Therefore, a reasonable measure of comparison, between the numerical and experimental results, could be the spectral separation between orthogonal polarizations under similar force loads [6]. During the experiment, the evolution of the reflected peaks, for both polarisation axes, was followed with the increasing of the transverse load, specially, in fig.5b became to be the main peaks. The results of the comparisons are presented in Table 1.

Table 1. Difference between the wavelengths of the Bragg peaks of the experiment and the simulation.

Transverse load		2 [N]	5 [N]	20 [N]
Experiment	$\lambda_{B_x} - \lambda_{B_y}$ [nm]	0.128	0.108	0.34
Simulation	$\lambda_{B_x} - \lambda_{B_y}$ [nm]	0.108	0.16	0.324

Furthermore, the oscillations in the reflection spectra increase in amplitude. Our hypothesis is that the inherent anisotropy of the optical fibre's core in real sensors under transverse forces enhances the amplitude of the higher order modes in the reflection spectra, which projects itself as higher frequency oscillating waves in the reflection spectra. This phenomenon can be noted in Fig. 5b, where the wavelength range has been kept broader than the Fig. 5a to show the increasing of the oscillations on the sides of the reflected peaks with the growing of the transverse load. It is possible to point out that, in

this experiment, a further disturbance can originate of the edges at the steel block. If the edges are not sharp then the transverse load could be distributed non-uniformly on the FBG sensor but it would be loaded on the optical fibre, out from the FBG, generating the oscillations on the sides of the reflected peaks.

The second transverse load scenario that we discuss here is the FBG reflection spectra under a non-uniform transverse load. As described before, the tool used for transferring the load to the FBG sensor is a ball point bearing pin (80584 Alufix) with a sphere diameter of 6 mm. We show in Fig.6 the experimental setup for this scenario in which the pin is placed on the FBG and the Optoforce sensor is fixed to the base of the pin measuring the value of the load applied by the clamp. In this experiment, we cured the alignment between the elements of the setup so that the load was applied at the middle of the FBG sensor. It was observed that using cyanoacrylate to adhere the optical fibre to the aluminum surface results in a more brittle structure. Therefore, two sensors were used in this experiment to inspect this effect, one fibre adhered to the surface and one free standing. This allows the investigation of the effect of the glue layer on the FBG reflected spectrum since this could influence the load distribution on the optical fibre.

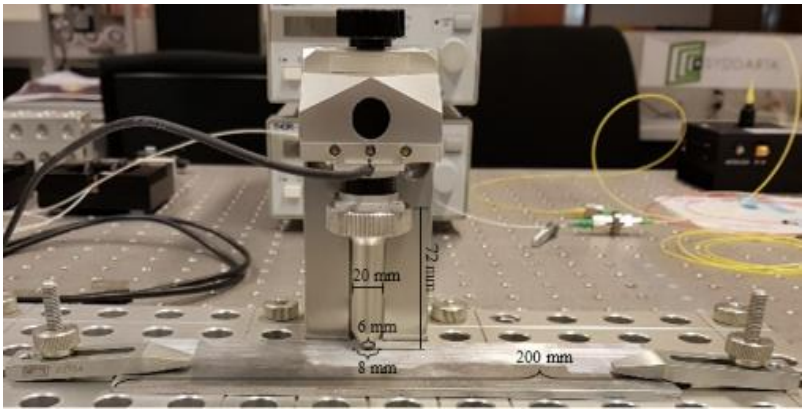

Fig. 6. Roll bearing pin experimental setup.

During the tests, it was observed that the glued FBG broke at 5 N, whereas the other FBG broke at around 8 N force. This brittleness was also seen in the way the sensors broke, in the glued sensor the ball bearing crushed the sensor (Fig.8a), while in the unmounted sensor it was cut (Fig.8b). The reflected spectra of the two cases are shown in the following figures, where it is possible to note that after breaking the sensor, the unglued sensor continued to function. Indeed, the Bragg peak is well-defined and placed approximately at the nominal Bragg wavelength, however the amplitude of the peak is low as after cutting the sensor has a lesser length. Instead, once the glued FBG was crushed it was not more able to reflect the light. This result is shown in figure 7a where the peak, for 5 N, is not defined as the sensor was insensitive to external perturbations.

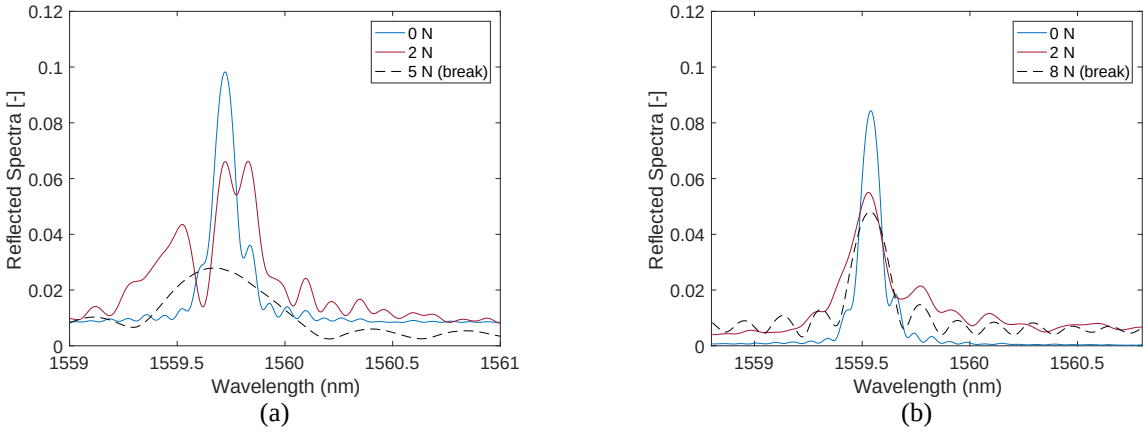

Fig. 7. Reflected spectra recorded for (a) experiment with roll bearing pin and a surface mounted FBG sensor and (b) the same experiment with the FBG sensor not mounted.

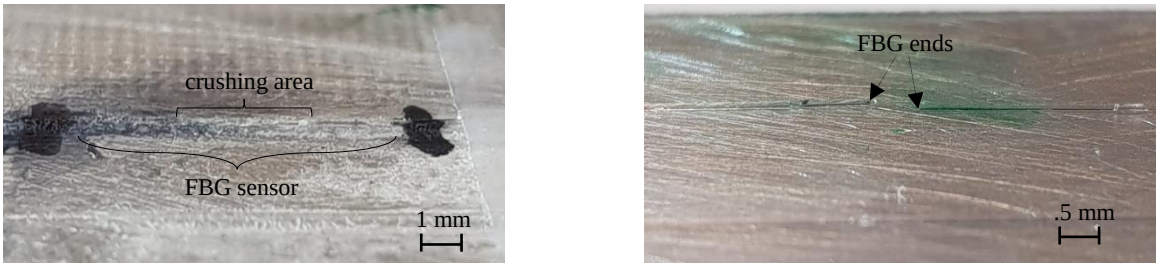

(a) (b)

Fig. 8. FBG failure: (a) crushing and (b) cutting.

Moreover, comparing the reflected spectra of the two FBGs, it can be seen that their shapes are also quite different for the same transverse load (2 N). We hypothesize that this behavior may depend on the different distribution of the load over the length of the sensor, since in the first case there is also an additional layer of cured cyanoacrylate on top of the sensor. To be more specific, the manual application of the cyanoacrylate on the sensor creates different thicknesses of the cured rigid adhesive over the length of the sensor. This difference in the thickness of the adhesive results in a non-uniform load transfer along the length of the sensor, which results in different reflected spectra in similar scenarios.

5. CONCLUSIONS

Due to transverse stresses and strains, the circular shape of the optical fibre's core changes, and the effective refractive indices across the two main polarization axes take different values. This causes birefringence, or the splitting of the main peak of the FBG reflection spectra into two or more peaks corresponding to the two main polarization axes. Increasing the transverse load the bifurcation of the main peak becomes more evident. Considering our model, the reflected peak related to the fast polarization axis is at a longer wavelength the to slow polarization axis. In this paper, we presented the transfer matrix model for analysis of FBG reflection spectra under uniform or non-uniform transverse loads. We presented computer simulations and experimental measurements to validate the model. The resulting reflected spectra were in agreement with the model in the fundamental feature, but quite different in their general morphology due to the issues related to the non-uniform load transfer of the cured adhesive. We studied the glue effect using a ball bearing pin to apply a non-uniform transverse load on a glued and a not glued FBG sensor. The reported results show two different failure modalities and behaviors in the spectra of the two sensors due to the different distribution of the load, and hence stress/strain state, over the length of the sensor.

6. ACKNOWLEDGEMENT

This research was performed in a collaboration between the University of Palermo and Delft University of Technology and was supported by the TKI Smart Sensing for Aviation Project, sponsored by the Dutch Ministry of Economic Affairs under the Topsectoren policy for High Tech Systems and Materials and the Operationeel Programma Zuid-Nederland (Op-Zuid) Project as part of the Dutch Composite Maintenance Centre (DCMC), supported by the Europees Fonds voor Regionale Ontwikkeling (EFRO).

REFERENCES

(1) D. Balageas, C.P. Fritzen, A. Guemes, ''Structural Health Monitoring,'' ISTE Ltd, first edition (2006).
(2) Y.J. Rao, ''Recent progress in applications of in-fibre Bragg grating sensor,'' Canterbury, Elsevier Science Ltd- UK, Optics and Lasers in Engineering 31, 297-324 (1999).
(3) C. Davis, S. Tejedor, I. Grabovac, J. Kopczyk, T. Nuyens, ''High-Strain Fibre Bragg Gratings for Structural Fatigue Testing of Military Aircraf,'' Photonic Sensors 2(3), 215-224 (2012).
(4) R. Gafsi, M. A. El-Sherif, ''Analysis of Induced-Birefringence Effects on Fibre Bragg Grating,'' Optical Fibre Technology, 6, 299-323 (2000).

(5) G. Chen, L. Liu, H. Jia, J. Yu, L. Xu, W. Wang, ''Simultaneous strain and temperature measurements with fibre Bragg grating written in novel Hi-Bi optical fibr,'' IEEE, Photonics Technology Letters, 16(1), 223 (2004).
(6) Y. Wang, B. Yun, N. Chen, Y. Cui, ''Characterization of a high birefringence fibre Bragg grating sensor subjected to non-homogeneous transverse strain fields,'' Meas. Sci. Technol., 17, (2006).
(7) R. Gafsi, A. Malki, F. Ahdad, P. Lecoy, J. Bures, ''Static stress optical-fibre sensor,'' Sensors and Actuators, A 62, 501-505 (1997).
(8) P.D. Gianino, B. Bendow, ''Calculations of stress-induced changes in the transverse refractive-index profile of optical fiber,'' Applied Optics, Vol.20, No.3, pp. 430-433, 1981.
(9) T. Erdogan, ''Fibre Grating Spectr,'' Journal of Lightwave Technology, Vol.15, No. 8, 1277-1294 (1997).
(10) M. Yamada, K. Sakuda, ''Analysis of almost-periodic distributed feedback slab waveguides via a fundamental matrix approach,'' Optical Society of America, 26(16), 3474-3478 (1987).
(11) A. Ikhlef, R. Hedara, M. Chikh-Bled, ''Uniform Fibre Bragg Grating modeling and simulation used matrix transfer metho,'' IJCSI International Journal of Computer Science Issues, 9(1), (2012).
(12) G. J. Liu, Q. Li, G. L. Jin, B. M. Liang, ''Transfer matrix method analysis of apodized grating coupler,'' Optics Communications, 235, 321 (2004).